Bulletin of the Seismological Society of America, Vol. 106, No. 2, pp. 673–686, April 2016, doi: 10.1785/0120150242

Evaluation of Six NEHRP B/C Crustal Amplification Models Proposed for Use in Western North America

by Kenneth W. Campbell and David M. Boore

Abstract We evaluate six crustal amplification models based on National Earthquake Hazards Reduction Program (NEHRP) B/C crustal profiles proposed for use in western North America (WNA) and often used in other active crustal regions where crustal properties are unknown. One of the models is based on an interpolation of generic rock velocity profiles previously proposed for WNA and central and eastern North America (CENA), in conjunction with material densities based on an updated velocity–density relationship. A second model is based on the velocity profile used to develop amplification factors for the Next Generation Attenuation (NGA)-West2 project. A third model is based on a near-surface velocity profile developed from the NGA-West2 site database. A fourth model is based on velocity and density profiles originally proposed for use in CENA but recently used to represent crustal properties in California. We propose two alternatives to this latter model that more closely represent WNA crustal properties. We adopt a value of site attenuation (κ_0) for each model that is either recommended by the author of the model or proposed by us. Stochastic simulation is used to evaluate the Fourier amplification factors and their impact on response spectra associated with each model. Based on this evaluation, we conclude that among the available models evaluated in this study the NEHRP B/C amplification model of Boore (2016) best represents median crustal amplification in WNA, although the amplification models based on the crustal profiles of Kamai *et al.* (2013, 2016, unpublished manuscript, see Data and Resources) and Yenier and Atkinson (2015), the latter adjusted to WNA crustal properties, can be used to represent epistemic uncertainty.

Introduction

Boore and Joyner (1997) (hereafter referred to as BJ97) developed shear-wave velocity and material density profiles for generic rock-site conditions in western North America (WNA). They used these profiles to develop ground-motion amplification factors relative to the material properties at the base of the crustal profile, which we refer to as crustal source properties, using the square-root impedance (SRI) approach described by Boore (2013). The SRI method is also known and referred to in the literature as the quarter-wavelength (QWL) method (Boore, 2003), which was first proposed by Joyner *et al.* (1981) as a means of incorporating site response in stochastic ground-motion simulations. The BJ97 amplification factors did not include the effects of attenuation within the profiles. This site attenuation is typically defined in terms of the spectral-decay parameter kappa (κ) and is often estimated by fitting the attenuation operator $\exp(-\pi\kappa f)$ to the observed Fourier amplitude spectrum (FAS), in which f is frequency (Hz) (Anderson and Hough, 1984; Campbell, 2009; Ktenidou *et al.*, 2014). Although κ will typically include the effects of both site attenuation and anelastic attenuation (Q), it is referred to as κ_0 when it is extrapolated to zero distance, in which it is usually assumed to be controlled by attenuation within the upper few kilometers of the crust (Boore, 2003; Campbell, 2009). It is relatively small for shallow hard-rock sites typical of central and eastern North America (CENA) crustal properties and is relatively large for deep soft-rock sites typical of WNA crustal properties (Campbell, 2009).

The BJ97 crustal amplification factors together with various values of κ_0 have been widely used to characterize the inferred crustal response included in WNA ground-motion prediction equations (GMPEs) when simulating ground motions using the point-source stochastic method of Boore (2005), the finite-source stochastic method of Motazedian and Atkinson (2005), and the hybrid empirical method (HEM) of Campbell (2003). Recent ground-motion models that have relied on WNA stochastic simulation are Atkinson and Silva (2000), Beresnev (2002), Beresnev and Atkinson (2002), Campbell (2003, 2004, 2007, 2011), Tavakoli and Pezeshk (2005), Pezeshk *et al.* (2011, 2015), Boore, Di Alessandro, Abrahamson (2014), Atkinson and Assatourians

(2015), and Yenier and Atkinson (2015), among others. The HEM used to develop GMPEs in CENA by Campbell (2003, 2004, 2007, 2011), Tavakoli and Pezeshk (2005), and Pezeshk *et al.* (2011, 2015) is sensitive to the crustal amplification model, because the HEM uses it to calculate adjustment factors needed to convert ground motions estimated by GMPEs from an active crustal region (ACR), such as WNA, to source and crustal conditions appropriate to the target region of low seismicity and different tectonic conditions, such as CENA, using the point-source stochastic method (Campbell, 2003, 2014).

The BJ97 generic rock WNA amplification factors were derived from a crustal profile with a time-averaged shear-wave velocity in the top 30 m (V_{S30}) of 618 m/s (often rounded to 620 m/s). This value is less than the value of $V_{S30} = 760$ m/s used to represent the reference site conditions in the U.S. National Seismic Hazard Maps (Petersen *et al.*, 2014) and used to define the reference site class for site factors included in the latest edition of the National Earthquake Hazards Reduction Program (NEHRP) provisions (Bonneville and Shuck, 2014; Building Seismic Safety Council, 2015; Luco *et al.*, 2015). Partly due to the use of an NEHRP B/C reference site condition in the development of the U.S. seismic hazard maps, this site condition has been adopted or recommended by some engineers and seismologists as the standard for evaluating GMPEs for site-specific site-response and seismic-hazard analyses (e.g., BC Hydro Engineering, 2012; Swissnuclear, 2013; Pacific Northwest National Laboratory, 2014; GeoPentech, 2015; R. Kamai *et al.*, unpublished manuscript, 2016; see Data and Resources). However, until recently there was no crustal amplification model available in the scientific literature that represented a WNA NEHRP B/C crustal profile. Walling *et al.* (2008) and Kamai *et al.* (2013) used an NEHRP B/C velocity profile to develop amplification factors for the Next Generation Attenuation (NGA)-West1 Project (Power *et al.*, 2008), but these factors have not generally been known or used in stochastic simulations. This oversight was corrected by Boore (2016; hereafter referred to as B16), who developed a $V_{S30} = 760$ m/s shear-wave velocity profile by interpolating the $V_S(z)$ profiles (in which z is depth) given in BJ97 for WNA generic rock ($V_{S30} = 618$ m/s) and CENA generic very hard rock ($V_{S30} = 2780$ m/s). B16 also used revised relationships for estimating material density (ρ) from V_S in the development of this new generic NEHRP B/C crustal profile.

There are also other available NEHRP B/C site profiles that have been used for various purposes to represent WNA crustal properties in past studies. One of these is the crustal model (consisting of both $V_S(z)$ and $\rho(z)$ profiles) developed by Frankel *et al.* (1996; hereafter referred to as Fea96) for use in CENA. The crustal amplification factors calculated from this model using the SRI approach have been used in several applications to represent WNA crustal properties. Frankel *et al.* (1996, 2002) and Petersen *et al.* (2008, 2014) originally used the Fea96 FAS crustal amplification factors together with a site attenuation parameter of $\kappa_0 = 0.01$ s to develop 5% damped pseudoacceleration response spectral (PSA) site factors that they used to adjust very-hard-rock (NEHRP A) ground motions estimated from CENA GMPEs to NEHRP B/C site conditions. Atkinson and Boore (2006) used the Fea96 amplification factors, adjusted to represent slightly different values of shear-wave velocity and density at the base of the profile, together with a site attenuation parameter of $\kappa_0 = 0.02$ s to represent NEHRP B/C site conditions in a CENA GMPE that they developed using the finite-source stochastic simulation program EXSIM (Motazedian and Atkinson, 2005; Atkinson *et al.*, 2009; Boore, 2009; Atkinson and Assatourians, 2015). The reason Fea96 is included in this discussion of WNA crustal models is because Yenier and Atkinson (2015) used the same amplification factors as Atkinson and Boore (2006), but with a site attenuation parameter of $\kappa_0 = 0.025$ s, to develop an equivalent point-source seismological model for California to use with the stochastic simulation program SMSIM (Boore, 2005).

To be thorough, we also evaluate the Walling *et al.* (2008) and Kamai *et al.* (2014) WNA NEHRP B/C crustal profiles that were used as one of their base profiles for developing nonlinear ground-motion amplification factors for the NGA-West1 Project (Power *et al.*, 2008) and the NGA-West2 Project (Bozorgnia *et al.*, 2014) using 1D equivalent-linear site-response analyses. These profiles were based on velocity measurements obtained primarily in the upper 100 m of the site and, in the case of the Walling *et al.* (2008) profile, were merged with the BJ97 WNA generic rock profile at depth. The $V_S(z)$ profile used by Kamai *et al.* (2014) is plotted in Kamai *et al.* (2013; hereafter referred to as Kea13) and was provided in digital form by R. Kamai and W. J. Silva (see Data and Resources). Kea13 constrained the linear damping in their site-response analyses to be consistent with a total crustal profile attenuation corresponding to $\kappa_0 = 0.04$ s. We used Kea13 in this study because it represents an updated version of the study done by Walling *et al.* (2008). R. Kamai *et al.* (unpublished manuscript, 2016, [KEA16]; see Data and Resources) used site data from the final NGA-West2 database (Ancheta *et al.*, 2014; Seyhan *et al.*, 2014) to derive an updated shear-wave velocity profile for sites with $V_{S30} = 760$ m/s in California and Japan. They suggest that their California profile is an updated version of that used by Kea13, but, because Kea13 is the current basis of the site profile used to develop nonlinear site factors for the NGA-West2 Project, we decided to retain both site profiles in our study. Besides, Kea16 is based only on measured $V_S(z)$ profiles in California and cannot be extended reliably below about 100 m (R. Kamai, personal comm., 2015). To overcome this limitation, we merged the Kea16 California profile with that of B16 below 120 m and adopted the same value of κ_0 used in Kea13 for purposes of calculating amplification factors.

As we show later, the amplification factors derived from the NEHRP B/C crustal models discussed previously in this article are very different, especially when differences in κ_0 recommended for use with these models by the authors of the models are taken into account. These differences motivated us to better understand the bases for these models

to evaluate their potential consequences on estimating surficial ground motions using the stochastic method. This was done by comparing crustal amplification from the four NEHRP B/C crustal models discussed previously, all of which have been used to characterize WNA crustal properties by various investigators. In addition, we also compare two models that we developed from the Fea96-based model used by Yenier and Atkinson (2015) in their California stochastic model to make it more consistent with WNA crustal properties. These crustal models have been most commonly used in stochastic ground-motion simulations in WNA, and to a more limited extent in other ACRs (e.g., Swissnuclear, 2013), that are intended to represent ground motions consistent with the NGA-West1 and NGA-West2 GMPEs, as well as GMPEs from other ACRs. Based on our evaluation, we recommend four NEHRP B/C amplification and crustal models that we believe can be used to represent epistemic uncertainty in WNA, especially when used to estimate the inferred crustal amplification in the NGA-West2 GMPEs when they are evaluated for $V_{S30} = 760$ m/s and default values of sediment depth. This is an important case to consider, because it was used by the National Seismic Hazard Mapping Project to develop the 2014 seismic hazard maps (Petersen *et al.*, 2014, 2015; Rezaeian *et al.*, 2014, 2015) and is similar to the $V_{S30} = 800$ m/s reference site conditions used to develop the 2012 European and Middle Eastern seismic hazard maps (Erdik *et al.*, 2012; Woessner *et al.*, 2012). It is also the reference site condition used as the basis for many major seismic design standards and building codes throughout the world (European Committee of Standardization, 2005; International Association for Earthquake Engineering, 2012; American Society of Civil Engineers, 2013; International Code Council, 2014; Building Seismic Safety Council, 2015). Furthermore, it has been used to define reference site conditions in several recent site-specific probabilistic seismic-hazard assessment projects (BC Hydro Engineering, 2012; Swissnuclear, 2013; Pacific Northwest National Laboratory, 2014; GeoPentech, 2015). R. Kamai *et al.* (unpublished manuscript, 2016; see Data and Resources) recommend $V_{S30} = 760$ m/s as the reference rock-site condition to use when evaluating NGA-West2 GMPEs for the development of bedrock ground motions used in site-specific site-response analyses.

NEHRP B/C Crustal Profiles

As indicated in the previous section, there are four $V_S(z)$ profiles that have been used to represent NEHRP B/C crustal models in WNA. The first is that of Fea96, with a modification by Atkinson and Boore (2006) to the values of V_S and ρ at the base of the profile at an 8 km depth (i.e., the crustal source properties β_S and ρ_S in the terminology of Boore, 2003), which was used by Yenier and Atkinson (2015) to develop a stochastic ground-motion model for California. The second is that of Kea13, which was used by Kamai *et al.* (2014) to develop a nonlinear site-response model to use in conjunction with the NGA-West2 GMPEs. This profile supersedes a similar profile used by Walling *et al.* (2008) to develop a nonlinear site-response model for the NGA-West1 GMPEs. The third velocity profile is that of Kea16, which was used to develop a parameterized model of $V_S(z)$ in terms of V_{S30} using California recording stations from the NGA-West2 site database (Ancheta *et al.*, 2014; Seyhan *et al.*, 2014). It was developed by taking the average value of V_S at a given depth for all of those profiles with a value of V_{S30} within 15% of the target value of 760 m/s. It actually has a calculated value of $V_{S30} = 772$ m/s, but we consider this value close enough to the 760 m/s target to be included in our study. The fourth is that of B16, which is intended to be an NEHRP B/C version of the WNA generic rock $V_S(z)$ profile of BJ97. It was developed by interpolating the BJ97 generic rock (WNA) and generic very-hard-rock (CENA) profiles for $V_{S30} = 760$ m/s. These four $V_S(z)$ profiles, along with the original BJ97 generic rock (BJ97gr) and generic very-hard-rock (BJ97gvhr) profiles are plotted in Figure 1 for reference. The $V_{S30} = 2.78$ km/s value

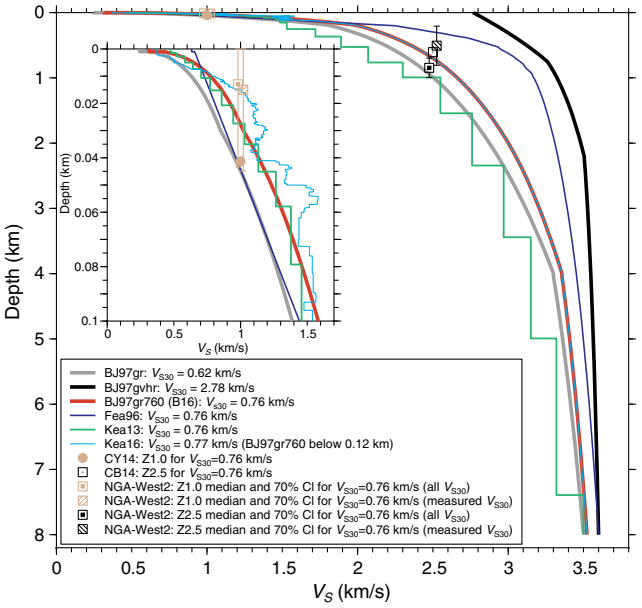

Figure 1. Shear-wave velocity as a function of depth for four proposed western North America (WNA) National Earthquake Hazards Reduction Program (NEHRP) B/C crustal profiles with $V_{S30} = 760$ m/s: BJ97gr760, profile developed by Boore (2016; referred to as B16); Fea96, Frankel *et al.* (1996); Kea13, Kamai *et al.* (2013); and Kea16, R. Kamai *et al.* (unpublished manuscript, 2016; see Data and Resources). The generic rock (BJ97gr) and generic very hard-rock (BJ97gvhr) profiles of Boore and Joyner (1997) are also shown for reference. The points and bars are the medians and 70% median confidence intervals (CI) of $Z_{1.0}$ and $Z_{2.5}$ for sites with measured and measured-plus-estimated values of $V_{S30} \approx 760$ m/s from the Next Generation Attenuation (NGA)-West2 site database (the V_S values of the points have been offset slightly for plotting purposes to eliminate overlap). The points without bars are default values of $Z_{1.0}$ and $Z_{2.5}$ predicted from V_{S30} using relationships developed by Chiou and Youngs (2014) (CY14) and Campbell and Bozorgnia (2014) (CB14) with data from the NGA-West2 site database. The color version of this figure is available only in the electronic edition.

Table 1
Summary of Western North America (WNA) NEHRP B/C Crustal Amplification Models

Amplification Model	$V_S(z)$ Profile	$\rho(z)$ Profile	β_S (km/s)	ρ_S (g/cm^3)	κ_0 (s)
B16	BJ97gr760	B16	3.5	2.72	0.034, 0.44
Fea96mod1*	Fea96	Fea96	3.7	2.80	0.025
Fea96mod2	Fea96	Fea96	3.5	2.72	0.025
Fea96mod3	Fea96	B16	3.5	2.72	0.025
Kea13	Kea13	B16	3.5	2.72	0.040
Kea16	Kea16, BJ97gr760†	B16	3.5	2.72	0.040‡

BJ97gr760, profile developed by Boore (2016; referred to as B16); Fea96, Frankel *et al.* (1996); Kea13, Kamai *et al.* (2013); Kea16, R. Kamai *et al.* (unpublished manuscript, 2016; see Data and Resources); $V_S(z)$ and $\rho(z)$, shear-wave velocity and material density versus depth (z); β_S and ρ_S, crustal source properties at a reference depth of 8 km. NEHRP, National Earthquake Hazards Reduction Program.

*Amplification model used by Atkinson and Boore (2006) and Yenier and Atkinson (2015).

†Uses Kea16 $V_S(z)$ profile for $z \leq 120$ m and BJ97gr760 $V_S(z)$ profile for $z > 120$ m.

‡Adopted from Kea13.

attributed to the BJ97gvhr velocity profile corrects a typographical error in the value of 2.88 km/s that was originally reported in Boore and Joyner (1997).

The $V_S(z)$ profile used in the B16 crustal model is referred to in Figure 1 as BJ97gr760 (Boore, 2016) to identify it as having been derived from the BJ97gr and BJ97gvhr $V_S(z)$ profiles. Figure 1 shows that the Kea13 and BJ97gr760 profiles are very similar in the upper 100 m, aside from the fact that the Kea13 profile is stepped (layered) rather than smoothly varying with depth. On the other hand, the Kea16 profile has a slightly steeper velocity gradient than BJ97gr760 or Kea13 in the upper 50 m, and the Fea96 profile has a weaker velocity gradient than the other three profiles in the upper 30 m. The BJ97gr760, Kea13, and Fea96 profiles are notably different at larger depths, where Fea96 has a much steeper velocity gradient than the other two and BJ97gr760 has a somewhat steeper velocity gradient than Kea13 to depths of around 5 km. Kea16 shares the same velocity model as BJ97gr760 below 120 m. The steeper velocity gradient and shallower depth to high crustal velocities and densities exhibited by the Fea96 profile are fundamental properties of CENA crustal properties that distinguishes them from typical WNA crustal properties. Differences in these velocity gradients and the use of a coarsely layered profile by Kea13 can significantly impact ground-motion amplification, as we show in the NEHRP B/C Crustal Amplification section.

The Fea96 and B16 crustal models have density profiles associated with them. However, Kea13 does not report the densities they used to develop their nonlinear site-amplification model. For that reason, the development of crustal amplification factors for the Kea13 model discussed in the next section uses densities estimated from the updated V_S–ρ relationship of B16. Shown in Figure 1, and discussed later in the article, are the depths to the 1.0 km/s shear-wave velocity horizon ($Z_{1.0}$) and the 2.5 km/s shear-wave velocity horizon ($Z_{2.5}$) for a site with $V_{S30} \approx 760$ m/s that we derived from the NGA-West2 site database (Ancheta *et al.*, 2014; Seyhan *et al.*, 2014). Figure 1 also shows the values of $Z_{1.0}$ and $Z_{2.5}$ recommended for use with the NGA-West2 GMPEs of Chiou and Youngs (2014; hereafter referred to as CY14) and Campbell and Bozorgnia (2014; hereafter referred to as CB14), respectively, by the authors of these GMPEs for $V_{S30} = 760$ m/s when the actual values of these sediment depths are unknown. Similar $Z_{1.0}$ default values were adopted by Abrahamson *et al.* (2014) and Boore, Stewart, *et al.* (2014) in the development of their NGA-West2 GMPEs. Idriss (2014) did not incorporate a sediment-depth term in his GMPE. A more complete discussion of these depths is presented in the Discussion and Conclusions sections.

NEHRP B/C Crustal Amplification

We use the four velocity profiles described in the previous section together with density profiles and site attenuation parameters proposed by the original authors, if available, to compare crustal amplification factors for the six crustal models summarized in Table 1. This table lists the source of $V_S(z)$ and $\rho(z)$ profiles and the values of the shear-wave velocity (β_S) and density (ρ_S) at the base of the profiles at a reference depth of 8 km that we used to calculate the crustal amplifications using the SRI approach. We chose this depth to represent the average depth to the earthquake source region in WNA.

We derive three sets of amplification models based on the Fea96 velocity profile to demonstrate the differences resulting from the use of different material densities, crustal source velocities, and crustal source densities. Fea96mod1 is the amplification model used by Yenier and Atkinson (2015) to develop their California stochastic ground-motion model and is the same one used by Atkinson and Boore (2006) to develop their CENA GMPE, which consists of the Fea96 velocity and density profiles with adjusted values of β_S, ρ_S, and κ_0 (Table 1). The Fea96mod2 amplification model uses the Fea96 velocity and density profiles but with values of β_S and ρ_S at the reference depth of 8 km proposed by B16 that are more appropriate for WNA crustal properties. The Fea96-mod3 amplification model uses the Fea96 velocity profile

together with B16 WNA crustal source properties (β_S and ρ_S) and densities from the B16 ρ–V_S relationships. These densities are an update to the older density model originally used in the development of the Fea96 crustal amplifications. Fea96mod2 and Fea96mod3 are intended to show the potential impact of using amplification factors from versions of the Fea96 crustal model that we consider to be more consistent with WNA crustal properties. In addition, Fea96mod3 shows the potential impact of using an updated density profile. The representative values of κ_0 associated with each of the crustal models given in the last column of Table 1 are discussed in the following section.

FAS Amplification Models

Amplification factors of FAS for all six amplification models were calculated using the SRI approach (Boore, 2013). The SRI calculation is based on the change in amplitude of waves within a ray tube that preserves a constant flux of energy (Joyner *et al.*, 1981). The amplification is given by the seismic impedance (equal to the product of velocity and density) at the earthquake source depth, which is assumed to be the depth to the bottom of the crustal profile (in our case, 8 km), divided by the effective seismic impedance of materials near the ground surface. This latter seismic impedance varies with frequency, because it represents an average of the velocity and density down to a depth of a QWL of vertically propagating shear waves of specified frequency. All of the amplification factors are based on the same set of frequencies used in B16 to facilitate their comparison. The B16 amplification factors are the same as those given in table 2 of Boore (2016). The amplification factors for a site attenuation parameter of $\kappa_0 = 0$ s are summarized in Table 2 and plotted in Figure 2a. The dashed lines for $f < 0.0886$ Hz in Figure 2 are used to indicate those frequencies for which it was necessary to extrapolate the 8-km-deep profiles to larger depths to calculate the amplification factors using the SRI method (Boore, 2013). This is because the QWLs of these frequencies are longer than the profile depth. To calculate the amplifications at these low frequencies, the depth of the profile was extended using the crustal parameters of the last layer (i.e., β_S and ρ_S).

To show the impact of κ_0 on the amplification factors, they were also calculated using values of κ_0 proposed for use with each of the crustal models by the original authors, when available. Because B16 did not recommend a specific value of κ_0, we adopted the minimum and maximum values of κ_0 implied by the high-frequency shape of the NGA-West2 GMPEs for a site with $V_{S30} = 760$ m/s, as determined by Zandieh *et al.* (2016; see Data and Resources) using the inverse random vibration theory approach of Al Atik *et al.* (2014). These values are $\kappa_0 = 0.034$ s for $\mathbf{M} < 4.3$ and $\kappa_0 = 0.044$ s for $\mathbf{M} > 5.7$. The lower end of this range is generally consistent with small-to-moderate-magnitude κ_0–V_{S30} data and predictive models for Japan, France, Switzerland, and worldwide (Silva *et al.*, 1999; Chandler *et al.*, 2006; Drouet *et al.*, 2010; Edwards *et al.*, 2011; Van Houtte *et al.*, 2011; Edwards, 2012; Poggi *et al.*, 2013), all of which are summarized in Poggi *et al.* (2013), Al Atik *et al.* (2014), Campbell *et al.* (2014), Hashash *et al.* (2014), and Ktenidou *et al.* (2014). It is also consistent with the average value of κ_0 used by Pezeshk *et al.* (2015) to represent WNA crustal conditions implied by the NGA-West2 GMPEs in the development of their HEM ground-motion model. The upper end of this range is generally consistent with moderate-to-large-magnitude estimates of κ_0 for $V_{S30} = 760$ m/s site conditions that are implied by the high-frequency spectral shapes of the NGA-West1 and NGA-West2 GMPEs and selected GMPEs from other ACRs worldwide (BC Hydro Engineering, 2012; Swissnuclear, 2013; Pacific Northwest National Laboratory, 2014; GeoPentech, 2015). Kea13 used a site attenuation parameter of $\kappa_0 = 0.04$ s to constrain the linear amplification factors implied by their California velocity profile. Kea16 did not recommend a specific value of κ_0; therefore, we adopted the same value of $\kappa_0 = 0.04$ s used by Kea13. Yenier and Atkinson (2015) used a site attenuation parameter of $\kappa_0 = 0.025$ s with their amplification model to estimate linear amplification factors for California. The FAS amplification factors associated with all of the κ_0 values were calculated by applying the attenuation operator $\exp(-\pi\kappa_0 f)$ to the FAS amplification factors in Table 2. They are plotted in Figure 2b.

Figure 2 clearly demonstrates the difference between the six FAS crustal amplification models. These differences

Table 2
Summary of Fourier Amplitude Spectra Amplification Factors ($\kappa_0 = 0$ s)

f (Hz)	B16	Fea96mod1	Fea96mod2	Fea96mod3	Kea13	Kea16
0.010	1.00	1.00	1.00	1.00	1.00	1.00
0.015	1.01	1.00	1.00	1.01	1.02	1.01
0.021	1.02	1.01	1.00	1.01	1.03	1.02
0.031	1.02	1.02	1.01	1.01	1.04	1.03
0.045	1.04	1.03	1.01	1.02	1.06	1.04
0.065	1.06	1.04	1.02	1.03	1.10	1.06
0.095	1.09	1.07	1.03	1.04	1.14	1.08
0.138	1.13	1.09	1.05	1.07	1.21	1.13
0.200	1.18	1.12	1.08	1.10	1.28	1.18
0.291	1.25	1.17	1.12	1.14	1.37	1.25
0.423	1.32	1.23	1.18	1.21	1.48	1.32
0.615	1.41	1.31	1.26	1.30	1.59	1.41
0.894	1.51	1.44	1.38	1.44	1.70	1.50
1.301	1.64	1.63	1.56	1.66	1.80	1.62
1.892	1.80	1.87	1.79	1.92	1.89	1.77
2.751	1.99	2.06	1.97	2.14	2.01	1.93
4.000	2.18	2.20	2.11	2.30	2.20	2.11
5.817	2.38	2.29	2.19	2.41	2.40	2.34
8.459	2.56	2.35	2.25	2.49	2.57	2.61
12.301	2.75	2.41	2.31	2.54	2.72	2.98
17.889	2.95	2.44	2.34	2.58	2.84	3.28
26.014	3.17	2.46	2.36	2.61	2.95	3.45
37.830	3.42	2.48	2.37	2.63	3.04	3.60
55.012	3.68	2.48	2.38	2.65	3.11	3.61
80.000	3.96	2.50	2.39	2.66	3.15	3.61

Amplification models are described in Table 1.

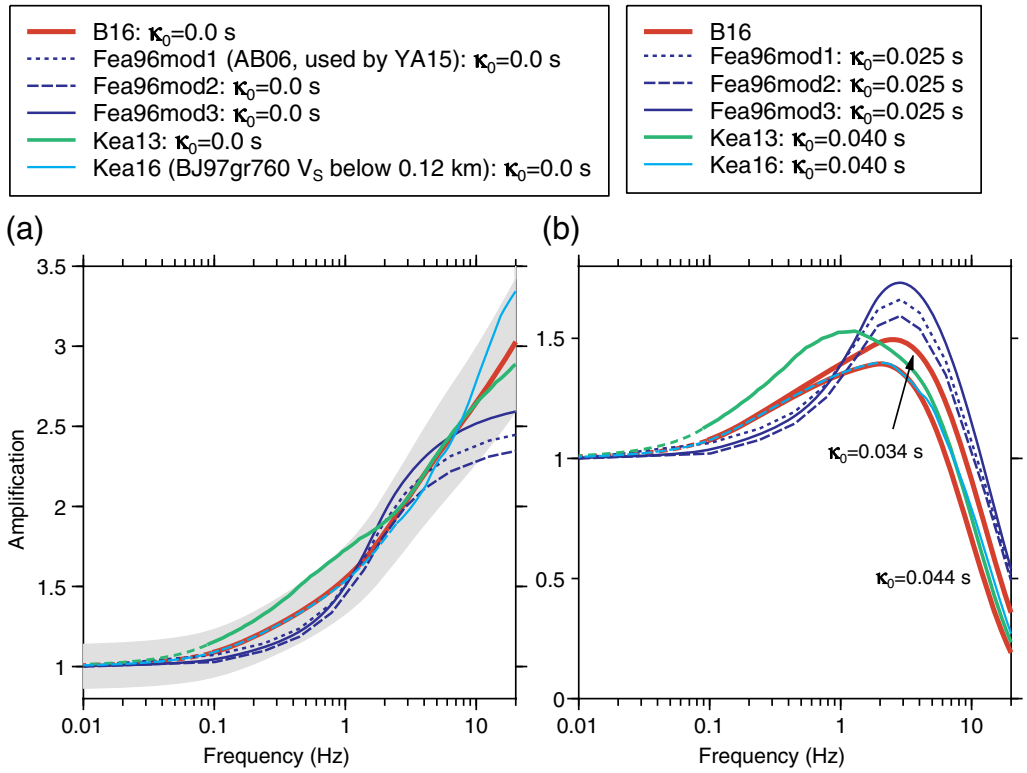

Figure 2. Fourier amplitude spectrum (FAS) amplification factors for four WNA NEHRP B/C (V_{S30} = 760 m/s) crustal profiles for (a) $\kappa_0 = 0$ s and (b) κ_0 equal to values recommended by the authors of the original studies or proposed in this study as listed in Table 1. The amplification models given in the legend are described in Table 1. The dashed lines at $f < 0.0886$ Hz indicate those frequencies for which it was necessary to extrapolate the 8-km-deep crustal profiles of B16, Kea13, and Kea16 to larger depths to calculate the amplification factors using the square-root impedance (SRI) method. The dashed line for Kea16 represents those amplification factors that are based on the B16 crustal profile for depths below 120 m. Abbreviations are given in the caption to Figure 1. The color version of this figure is available only in the electronic edition.

manifest themselves in terms of variations in both spectral shape and spectral amplitude and impact the entire frequency range of engineering interest, generally assumed to be f = 0.1–10 Hz (T = 0.1–10 s, in which T is spectral period). Figure 2a compares the FAS amplification factors, excluding site attenuation, associated with the five NEHRP B/C crustal profiles. At $f < 2$ Hz, Kea13 exhibits the highest amplification factors and the Fea96 models exhibit the lowest, with B16 and Kea16 (Kea16 is similar to the B16 model at these frequencies) falling in between the two. At high frequencies, the amplitudes of the amplification factors are in reverse order, with Kea16 being the highest at $f > 8$ Hz. The shaded area envelopes the amplification factors of the Kea13 (highest) and Fea96mod3 (lowest) for frequencies of general interest ($f < 20$ Hz). We believe that this envelope represents a reasonable estimate of epistemic uncertainty. We did not include the Fea96mod1 and Fea96mod2 models in determining this envelope, because we believe that the updates made to Fea96mod3 make it more appropriate for use in WNA. Nonetheless, these two models fall within the shaded region for $f < 10$ Hz. This region represents amplifications that are factors of 1.13 and 0.86 around the intermediate amplification factors of B16.

Figure 2b shows the same amplification factors as in Figure 2a, except modified by the attenuation operator. At low frequencies, which are not impacted by the attenuation operator, the comparison is similar to Figure 2a. However, there are significant differences at high frequencies. The relative amplitudes of the amplification models reverse order at $f > 1.2$ Hz, compared with the models with $\kappa_0 = 0$ s, such that now the highest amplification factors are for the Fea96-mod models, which have the smallest values of κ_0, and the lowest amplification factors are for the Kea13 and B16 models (the latter for $\kappa_0 = 0.044$ s), which have the largest values of κ_0. The B16 model, with a site attenuation parameter of $\kappa_0 = 0.034$ s, has amplification factors that are intermediate to the smaller factors of B16 with $\kappa_0 = 0.044$ s, Kea13, and Kea16 and to the larger factors of the Fea96mod models. The difference in the Kea13 and Kea16 amplification factors at high frequencies still exists (it appears to have disappeared, but this is an illusion due to the steep slopes of the curves), but the effect of κ_0 is to reduce the amplitudes of the combined amplification and attenuation so that the differences are of no practical importance. We no longer include an envelope in the plot that incorporates κ_0, although we note that the effect of including the attenuation operator

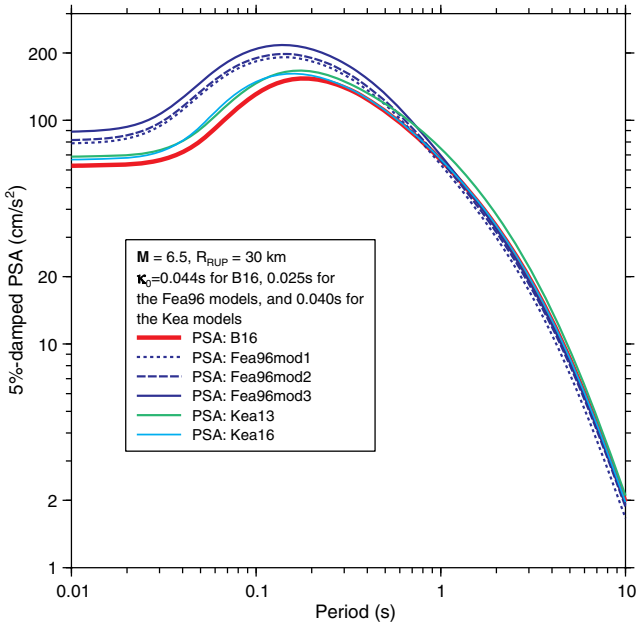

Figure 3. Response spectra predicted using SMSIM (Boore, 2005) and the stochastic model parameters listed in Table 3. The amplification models given in the legend are described in Table 1. The pseudoacceleration response spectra (PSA) predicted using the Kea13 and Kea16 amplification models almost appear to be identical at short periods because of the combined effects of amplification and attenuation within the profile that reduce these values to levels too small to be of practical interest. Abbreviations are given in the caption to Figure 1. The color version of this figure is available only in the electronic edition.

increases the variability of the amplification factors at high frequencies, thus serving as an additional source of epistemic uncertainty. The high-frequency FAS amplification factors are very sensitive to the exact value of κ_0 that is used. This latter point is demonstrated by the relatively large differences in the B16 amplification factors at $f > 1$ Hz that correspond to the two values of κ_0 used with this model. We do not necessarily believe that the specific values of κ_0 currently applied to some of these models will be those that are used in future applications, which is why we do not define a specific range in epistemic uncertainty. At high frequencies, the relatively large differences in the B16 amplification factors are a result of the differences in the mean site attenuation parameters of $\kappa_0 = 0.034$ s (corresponding to $\mathbf{M} < 4.3$) and $\kappa_0 = 0.044$ s (corresponding to $\mathbf{M} > 5.7$), which were derived from the NGA-West2 GMPEs by Zandieh *et al.* (2016; see Data and Resources). The incorporation of the between-model and within-model variability derived by Zandieh *et al.* (2016; see Data and Resources) would result in values of κ_0 that can be smaller or larger than these mean values.

Impact of FAS Amplification Models on PSA

To show the impact of the different crustal profiles and amplification models on 5% damped PSA, the stochastic simulation program SMSIM (Boore, 2005) was used together with the κ_0 values in Table 1 and the FAS amplification factors in Table 2 to calculate PSA (see Data and Resources). The stochastic model parameters that were used in the SMSIM ground-motion simulations are summarized in Table 3. They are typical of those used to represent seismological parameters in WNA (e.g., Campbell, 2003). In this case, a site attenuation parameter of $\kappa_0 = 0.044$ s was used with the B16 amplification model to be consistent with the relatively large magnitude of the scenario event. We use the term stress parameter rather than stress drop in Table 3 to be consistent with the terminology first proposed by Boore (1983). Simulations were done for an event with **M** 6.5 and a site located at $R_{\mathrm{RUP}} = 30$ km, in which R_{RUP} is represented by an equivalent point-source distance metric calculated using the finite-fault factor of Boore and Thompson (2015). The predicted response spectra are plotted in Figure 3.

Table 3
Stochastic Model Parameters Used to Evaluate the Crustal Amplification Factors

Parameter	Reference or Value
Source spectrum, $S(f)$	Brune (1970, 1971)
Source corner frequency, f_0 (Hz)	Brune (1970, 1971)
Crustal source parameters, β_S and ρ_S	Table 1
Stress parameter, $\Delta\sigma$ (bars)	100
Source duration, D_S (s)	$1/f_0$
Finite-fault factor	Boore and Thompson (2015)
Geometrical attenuation, $G(R)$	Raoof *et al.* (1999)
Anelastic attenuation, $Q(f)$	Raoof *et al.* (1999)
Path duration, D_P (s)	Boore and Thompson (2014)
Crustal amplification, Amp(f)	Table 2
Site attenuation, κ_0 (s)	Table 1

Figure 3 shows the variation in PSA from the six amplification models is no more than 20% at mid-to-long periods, with Kea13 giving the highest values and Fea96mod1 the lowest values. The differences at short periods are more significant, being as much as a factor of 2, with Fea96mod3 giving the highest values and B16 giving the lowest values, because of the relatively large value of κ_0 used with this latter model. Kea13 and Kea16 give virtually identical short-period estimates of PSA compared to those for FAS due to the strong impact of κ_0 (the 16% differences in the FAS at 20 Hz are now 3% differences in PSA at $T = 0.01$ s). Figure 3 shows that the short-period amplitudes of PSA are very sensitive to the specific characteristics of the FAS amplification model, especially the value of κ_0, and that care should be taken when selecting an appropriate value for this site attenuation parameter. The trends shown in Figure 3 are similar to those exhibited by the FAS amplification factors in Figure 2. The revised densities used with the Fea96mod3 amplification model result in 10%–15% higher short-period estimates of PSA compared with the older densities used with the Fea96-mod2 model. These differences are larger than the 5% differences at short-to-mid periods caused by the CENA-like values of β_S and ρ_S used by Yenier and Atkinson (2015) in

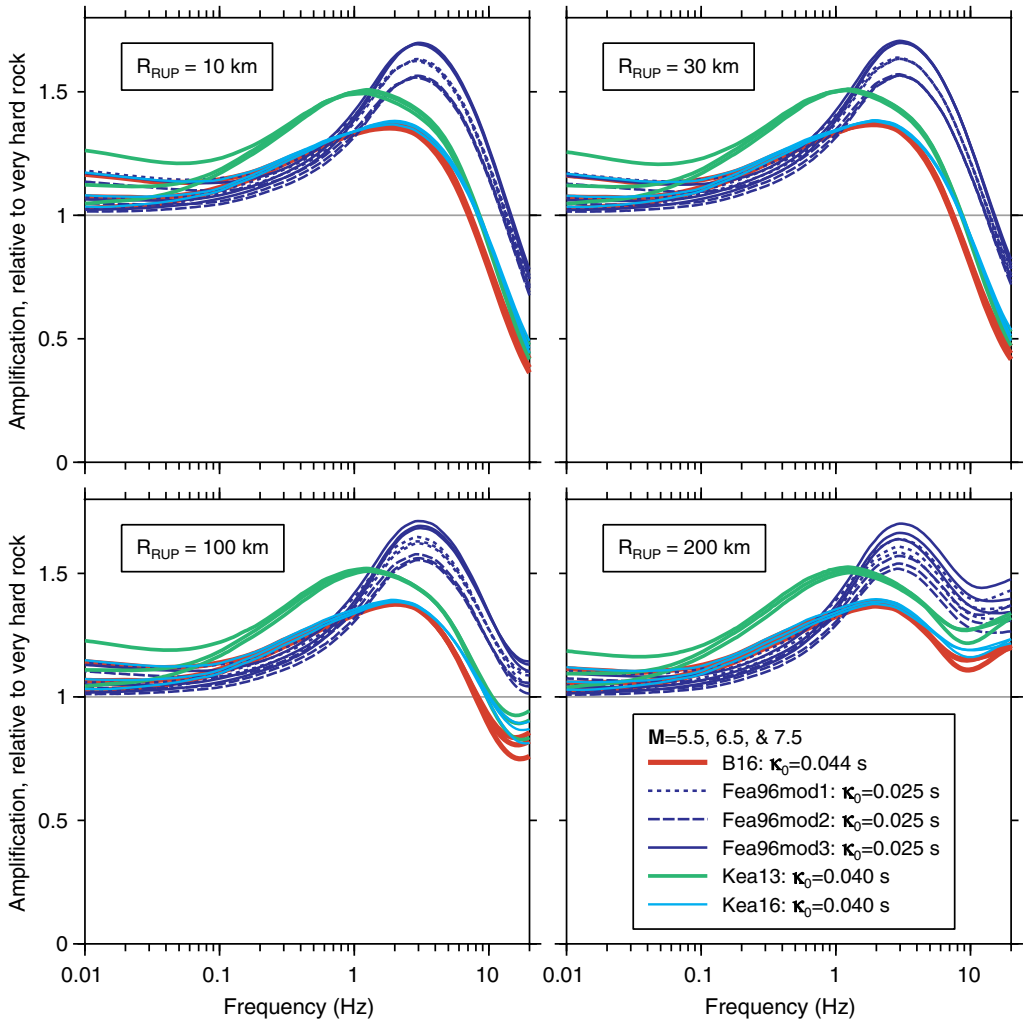

Figure 4. Ratios of response spectra calculated using the crustal amplification models listed in Table 1 and the κ_0 values given in the legend with respect to spectra calculated for very hard rock with $\kappa_0 = 0$ s. The spectra were calculated with SMSIM (Boore, 2005) using the stochastic model parameters listed in Table 3. Ratios are shown for **M** 5.5, 6.5, and 7.5 and $R_{\mathrm{RUP}} = 10$, 30, 100, and 200 km. The ratios clearly show the influence of the velocity profile, site attenuation, and distance on the amplification predicted by the models. Abbreviations are given in the caption to Figure 1. The color version of this figure is available only in the electronic edition.

the Fea96mod1 model compared with the WNA-like values used in the Fea96mod2 model but are similar to those of the Fea96mod2 model at longer periods.

Figure 4 shows the effect of magnitude for **M** 5.5, 6.5, and 7.5 and distance for $R_{\mathrm{RUP}} = 10$, 30, 100, and 200 km on estimates of PSA obtained from the stochastic simulations. All other stochastic parameters are the same as in Table 3. In this case, we have taken the ratio of the value of PSA that includes the effects of both amplification and κ_0 with respect to estimates of PSA that exclude these effects (i.e., the spectral values expected on very hard rock with crustal properties the same as those at the base of the crustal profile). This ratio is roughly the response-spectral equivalent to FAS amplification in the Fourier spectral domain. In general, the impact of magnitude is relatively small. It becomes more important, but still less than 10%, at low and high frequencies due to the unique characteristics of PSA to asymptotically approach peak ground acceleration (PGA) at high frequencies and peak ground displacement (PGD) at low frequencies (Gupta, 1993), together with the related complex relationship of PSA with magnitude, distance (attenuation), amplification, and oscillator response at these frequencies. At high frequencies, the ratio reaches a minimum as PSA asymptotically approaches the value of PGA. This minimum shifts to smaller frequencies as distance increases (this minimum occurs at $f > 20$ Hz at short distances and does not appear in Fig. 4). The flattening or slight upward trend of the ratio at long periods ($f < 0.2$ Hz, $T > 5$ s) occurs as PSA is controlled by the relative displacement of the oscillator, which approaches the value of PGD at long periods. At these long periods, the smaller-magnitude events have larger ratios than the larger-magnitude events, because the value of PGD corresponds to a

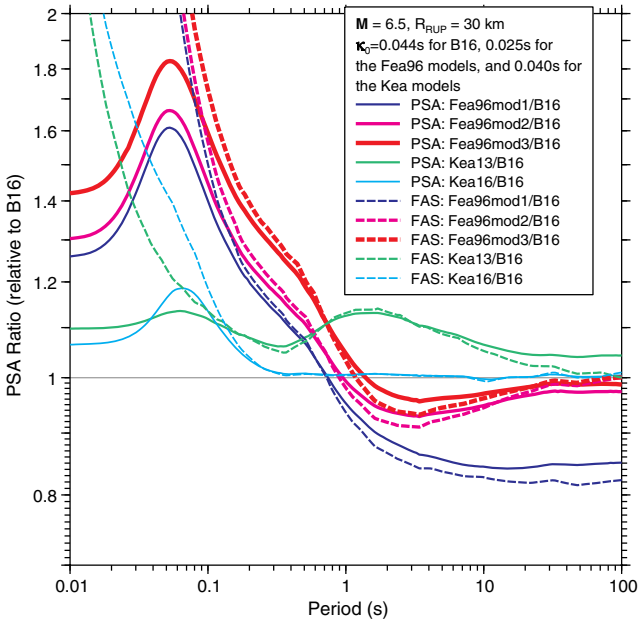

Figure 5. Ratios of Fourier amplitude and response spectra calculated using the crustal amplification models listed in Table 1 and the κ_0 values given in the legend with respect to the amplification model of B16. The spectra were calculated with SMSIM (Boore, 2005) using the stochastic model parameters listed in Table 3. Ratios are shown for **M** 6.5 and $R_{RUP} = 30$ km. The ratios clearly show the influence of the different velocity profiles and site attenuation on the relative amplification predicted by the models, and they demonstrate the difference between PSA and FAS, especially at short periods. Abbreviations are given in the caption to Figure 1. The color version of this figure is available only in the electronic edition.

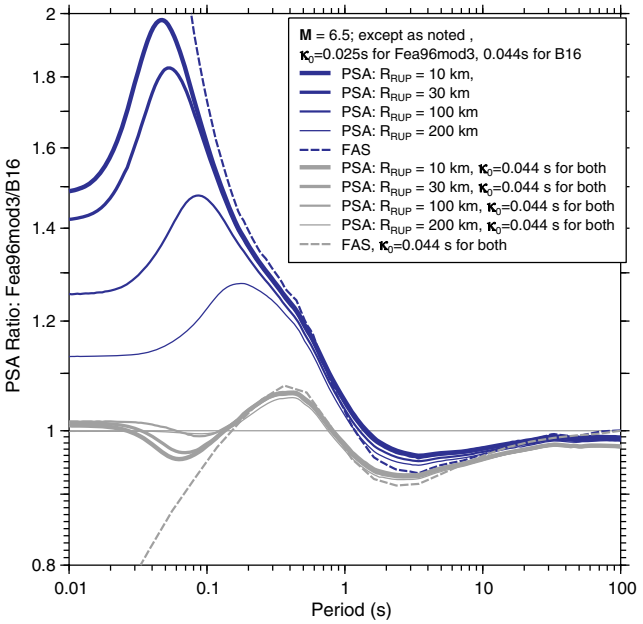

Figure 6. Ratios of Fourier amplitude and response spectra calculated using the crustal amplification model of Fea96mod3 and the κ_0 values given in the legend with respect to the amplification model of B16. The spectra were calculated with SMSIM (Boore, 2005) using the stochastic model parameters listed in Table 3 and amplification models listed in Table 1. Ratios are shown for **M** 6.5 and $R_{RUP} = 10$, 30, 100, and 200 km. The ratios clearly show the influence of velocity profiles, site attenuation, and distance on the relative amplification predicted by the two models, and they demonstrate the difference between PSA and FAS, especially at short periods. Abbreviations are given in the caption to Figure 1. The color version of this figure is available only in the electronic edition.

higher frequency and is, therefore, amplified more strongly by the crustal profile.

The asymptotic behavior of the PSA ratios and how they differ from equivalent ratios of FAS for each of the crustal amplification models are shown in Figure 5 for an event with **M** 6.5 and $R_{RUP} = 30$ km. For this purpose, we take ratios with respect to the B16 amplification model to better show relative differences among the six models. Although ratios could be calculated with respect to any one of the models, the B16 model with a site attenuation parameter of $\kappa_0 = 0.044$ s was chosen because we recommend its amplification factors as being most representative of a WNA NEHRP B/C profile for reasons presented in the Discussion section. Amplitudes of FAS and PSA were calculated using SMSIM with the stochastic model parameters summarized in Table 3.

The ratios given in Figure 5 clearly show the departure in behavior between FAS and PSA at high frequencies (short periods) due to the varying contribution of high-frequency ground motions on the amplitude of PSA at periods below the peak (T_P) in the response spectrum, which according to Figure 3 corresponds to periods in the range $T_P = 0.15$–0.2 s. As Douglas and Boore (2011), Scherbaum *et al.* (2011), and Boore and Goulet (2014) demonstrate, the amplitude of PSA at a given period T_0 shorter than the peak in the response spectrum ($T_0 < T_P$) includes contributions from periods $T > T_0$ due to the unique properties of the response of a damped oscillator to a specific input ground motion. The FAS does not exhibit this characteristic. The differences in the PSA and FAS ratios at long periods are due to the differences between ground motions and oscillator response in the displacement domain of the PSA. These results clearly show why FAS amplification factors should not be used to adjust response spectra for site effects. These ratios also show that the predicted PSA of the five crustal amplification models relative to B16 can be as high as a factor of 1.8 at short periods and as little as 0.8 at long periods.

Figure 6 shows the FAS and PSA ratios between the Fea96mod3 and B16 amplification models for an event with **M** 6.5 and a site at $R_{RUP} = 10$, 30, 100, and 200 km. Fea96-mod3 was used for this purpose because it emphasizes the potentially strong impact that κ_0 can have on the relative difference in the predicted value of PSA, depending on the amplification model that is used. The dark solid lines demonstrate the effect of differences in PSA when the recommended site attenuation parameter of $\kappa_0 = 0.025$ s is used with the Fea96mod3 model and $\kappa_0 = 0.044$ s is used with B16. The ratio varies from a factor of nearly 2 at

$T = 0.045$ s ($f = 22$ Hz) and $R_{RUP} = 10$ km to nearly 1.3 at $T = 0.15$ s ($f = 7$ Hz) and $R_{RUP} = 200$ km. These differences are much less at long periods. The gray solid lines show that the high-frequency differences reduce substantially when the same site attenuation parameter of $\kappa_0 = 0.044$ s is used with both amplification models. The dashed lines show similar ratios for FAS, which are independent of distance, but strongly dependent on the assumed values of κ_0.

Discussion

The main result of this study is the comparison and evaluation of the six FAS crustal amplification models presented in Figure 2a. This figure shows that these amplification factors can vary by several tens of a percentage. The amplification factors that include the effects of κ_0, shown in Figure 2b, have even larger variations at short periods, depending on the value of κ_0 that is used. We selected values of κ_0 that were either proposed by the original authors of the crustal models (Fea96mod1 and Kea13) or, if none were proposed, that were used by the authors in a similar model (Kea16) or derived directly from the NGA-West2 GMPEs (B16). The Fea96mod2 and Fea96mod3 models are perturbations of the Fea96mod1 model that use updated crustal source properties, which in our opinion are more appropriate to WNA crustal properties, together with either the original density profile of Fea96 (Fea96mod2) or a revised density profile based on the new velocity–density relationship in B16 (Fea96mod3). The B16 model demonstrates the impact of using two different values of κ_0 derived from the high-frequency shapes of the NGA-West2 GMPEs by Zandieh *et al.* (2016, see Data and Resources) for $\mathbf{M} < 4.3$ ($\kappa_0 = 0.034$ s) and $\mathbf{M} > 5.7$ ($\kappa_0 = 0.044$ s). Figure 3 shows the sensitivity of PSA response spectra to the six amplification models. The complex way that the amplification models impact estimates of FAS and PSA are demonstrated in Figures 4–6. The behavior of PSA is particularly complex because of its tendency to become asymptotic to PGA at short periods and to PGD at long periods. Because of these complexities, FAS amplification factors should not be used to adjust PSA for site-amplification effects, particularly at short periods.

Having evaluated comparisons among the six FAS crustal amplification models, the question that remains is, what NEHRP B/C crustal amplification model is most appropriate for stochastic ground-motion simulations in WNA, especially if this model is intended to represent the crustal profile inherent in the NGA-West2 GMPEs? To begin with, we eliminate the amplification factors based on the Fea96 NEHRP B/C velocity profile (Fea96mod1, Fea96mod2, and Fea96mod3) as being the most appropriate, because, although this profile was originally developed from a WNA velocity profile, it was adjusted to have a velocity gradient that is more representative of CENA crustal properties (Frankel *et al.*, 1996). The B16, Kea13, and Kea16 amplification factors are all derived from shear-wave velocities that are based on geotechnical measurements of $V_S(z)$ in the upper 30–100 m, largely from California, and on estimates of $V_S(z)$ from exploration geophysics and inversions of seismological data (sometimes estimated from compressional-wave velocities) in California and other parts of WNA at greater depths. This makes these models viable candidates for being the most appropriate NEHRP B/C amplification model in WNA, as represented by the NGA-West2 GMPEs. The B16 amplification model (without attenuation) is intermediate to those of the other candidate models, which makes it the obvious choice for the median model. However, to provide additional evidence in support of B16, we turn to the representative values of the sedimentary depths $Z_{1.0}$ and $Z_{2.5}$ for California sites with $V_{S30} \approx 760$ m/s. This brings us back to Figure 1.

Evaluation of Sediment Depths in the NGA-West2 Database

Figure 1 displays the median (default) values of $Z_{1.0}$ and $Z_{2.5}$ for a site with $V_{S30} = 760$ m/s, predicted from the $Z_{1.0}$–V_{S30} relationship of CY14 and the $Z_{2.5}$–V_{S30} relationship of CB14. A plot of $Z_{2.5}$ versus V_{S30}, given in Campbell and Bozorgnia (2013), demonstrates that the dispersion in these predicted values is large and, because the majority of the data is for $V_{S30} < 760$ m/s, might not be representative of average NEHRP B/C site conditions. To overcome this potential limitation, we extracted a list of all of the California recording stations for which both values of $Z_{2.5}$ and V_{S30} are available from the NGA-West2 site database (Ancheta *et al.*, 2014; Seyhan *et al.*, 2014), and we then calculated the median value of $Z_{2.5}$ and its associated confidence limits for values of V_{S30} around the target value of 760 m/s. The median (the point of a distribution at which the number of data on each side of the median is equal), rather than the mean was used to represent the central tendency of $Z_{2.5}$; the mean represents a robust alternative to the mean, because it is little influenced by outliers (Harding *et al.*, 2014). The initial target range of 760 m/s ± 10% had to be adjusted slightly and extended on the upper end to find a range that had a mean V_{S30} at or near 760 m/s. We refer to this median as $\tilde{Z}_{2.5}$, using the notation of Harding *et al.* (2014).

To find the variability of $\tilde{Z}_{2.5}$, we calculated its confidence interval (CI) from the equation (Harding *et al.*, 2014):

$$\mathrm{CI}_{1-\alpha} = \tilde{Z}_{2.5}\mathrm{SE}_{\mathrm{MD}}t_{n-1}(\alpha/2, 1-\alpha/2), \qquad (1)$$

in which α is the confidence level, $100(1-\alpha)$ is the CI as a percentage (e.g., $\alpha = 0.05$ for a CI of 95%), $\mathrm{SE}_{\mathrm{MD}}$ is the standard error of the median depth, and $t_{n-1}(\alpha/2, 1-\alpha/2)$ is the critical value from the Student's t distribution for a confidence level of α. The standard error of the median depth was calculated from the equation (Harding *et al.*, 2014):

$$\mathrm{SE}_{\mathrm{MD}} = 1.253\frac{\sigma}{\sqrt{n}}, \qquad (2)$$

in which σ is the standard deviation of $Z_{2.5}$, n is the number of values, and $\sigma/\sqrt{n}$ is the standard error of the mean. We

Table 4
Statistical Analysis of Sediment Depths for California Sites in the NGA-West2 Site Database with $V_{S30} \approx 760$ m/s

	$Z_{1.0}$ (km)		$Z_{2.5}$ (km)	
Statistic	All V_{S30}	Measured V_{S30}	All V_{S30}	Measured V_{S30}
Number of values	60	27	55	22
Range of V_{S30} (m/s)	684–895	660–874	684–1016	660–969
Mean V_{S30} (m/s)	759	762	762	760
Median V_{S30} (m/s)	760	760	760	733
Mean depth	0.104	0.0784	0.844	0.760
Median depth	0.0130	0.0150	0.846	0.507
Standard error of median depth	0.0290	0.0284	0.142	0.283
70% median CI	0–0.0434	0–0.0448	0.697–0.995	0.207–0.807
80% median CI	0–0.0507	0–0.0519	0.662–1.030	0.134–0.880
90% median CI	0–0.0614	0–0.0624	0.609–1.083	0.020–0.994
95% median CI	0–0.0710	0–0.0718	0.563–1.130	0–1.093

CI, confidence interval; NGA, Next Generation Attenuation.

calculated statistics for all of the available values of $Z_{2.5}$ and separately for those values of $Z_{2.5}$ from sites where V_{S30} was measured. This is important because only 23% of the California stations that we selected had measured values of V_{S30}. The rest of the values were estimated from geological and geophysical proxies presented in Seyhan *et al.* (2014). The same procedure was used to calculate median values and median CIs of $Z_{1.0}$ for sites with $V_{S30} \approx 760$ m/s. In this case, 24% of the California stations that we selected had measured values of V_{S30}. The statistical results for both sediment depths are listed in Table 4 for median CIs of 70%, 80%, 90%, and 95%.

The medians and 70% confidence intervals (CI_{70}) of all (measured-plus-estimated) and measured values of $Z_{1.0}$ and $Z_{2.5}$ are plotted in Figure 1 for reference. The CI_{70} limits are plotted in this figure because it is approximately equal to the plus-and-minus one standard error bounds of the median estimates. There are several observations one can make from this plot. First, both of the median estimates of $Z_{1.0}$ fall close to one another and have almost equal CI_{70} limits. They are shallower than the default value of $Z_{1.0} = 0.041$ km predicted from the CY14 relationship. They are most consistent with those velocity profiles with steeper near-surface velocity gradients (BJ97gr760, Kea13, and Kea16). The Fea96 velocity profile and the predicted default value of $Z_{1.0}$ fall at the lower bound of the CI_{70} limits. Second, the median estimates of $Z_{2.5}$ are different from one another, although there is a significant overlap of their CI_{70} limits. Both sets of $Z_{2.5}$ CI_{70} limits include the velocity profiles of B16 (BJ97gr760) and Kea16, the latter of which is based on BJ97gr760 at that depth, and bracket the default value of $Z_{2.5} = 0.068$ km predicted from the CB14 relationship. Although these estimates are most consistent with the BJ97gr760 (B16) velocity profile, the Fea96 profile falls within the upper bound of the CI_{70} limits that are based on measured values of V_{S30}, and the Kea13 profile falls at the lower bound of the CI_{70} limits that are based on measured-plus-estimated values of V_{S30}. The central tendencies of the estimates of $Z_{1.0}$ and $Z_{2.5}$ plotted in Figure 1 taken *in toto* are most consistent with the BJ97gr760 velocity profile used in the B16 crustal model. Figure 2a also shows that the B16 crustal model has amplification factors that are intermediate to the three other amplification models (Fea96mod3, Kea13, and Kea16) that we consider to be viable candidates for NEHRP B/C site conditions representative of the NGA-West2 GMPEs. The amplification factors for these two profiles fall within 1.13 and 0.86 of the predicted B16 amplification factors for $f \leq 20$ Hz ($T \geq 0.05$ s). However, the large scatter in the statistical results of $Z_{1.0}$ and $Z_{2.5}$ and the increased uncertainty in predicted FAS amplification factors at high frequencies when site attenuation, represented by the spectral-decay parameter κ_0, is included through the attenuation operator of Anderson and Hough (1984) cannot rule out the other three viable amplification models. Of course, it cannot rule out other velocity profiles and amplification models that are yet to be developed for WNA or other ACRs as possible samples of the distribution of all possible generic NEHRP B/C sites.

Conclusions

Our comparison of amplification factors based on four viable NEHRP B/C crustal profiles that have been proposed to represent generic WNA crustal properties, and in some cases the crustal properties of other ACR regions, in the stochastic simulation of ground motion shows that their variation can be large due to differences in both velocity profiles and assumed values of κ_0. We realize that these differences can be mitigated by the adjustment of other stochastic model parameters (e.g., stress parameter and path duration) when the model is calibrated to actual recordings, as was done by Yenier and Atkinson (2015). However, such a calibration can distort these other parameters and limit their usefulness when extrapolating predicted ground motions outside of the range of data used for calibration. It is particularly important to use a stochastic model that matches seismological parameters inherent within the NGA-West2 GMPEs (Bozorgnia *et al.*, 2014) when adjusting these GMPEs to seismological

conditions that represent another tectonic environment, as is done in the HEM (Campbell, 2003, 2011, 2014).

Based on the results of this study, we believe that the NEHRP B/C WNA crustal profile and corresponding crustal amplification factors developed by Boore (2016) can be used to model the implied crustal properties in the NGA-West2 GMPEs of Abrahamson *et al.* (2014), Boore, Stewart, *et al.* (2014), Campbell and Bozorgnia (2014), Chiou and Youngs (2014), and Idriss (2014), when these GMPEs are evaluated for $V_{S30} = 760$ m/s reference site conditions and default values of sediment (basin) depth. The B16 FAS crustal amplification factors presented in Table 2 can be used as input to WNA stochastic simulation models to represent the ground-motion response of the crustal profile when site-specific information is not available. We also propose the use of the magnitude-dependent site attenuation parameters $\kappa_0 = 0.034$ s for $\mathbf{M} < 4.3$ and $\kappa_0 = 0.044$ s for $\mathbf{M} > 5.7$, developed by Zandieh *et al.* (2016; see Data and Resources) with the B16 FAS crustal amplification model, because they are consistent with the high-frequency shapes of the NGA-West2 GMPEs. However, we recognize that these values are subject to large variability and should be selected with caution. We have shown that κ_0 can impact predicted response spectra at high frequencies in complex ways due to the interaction of the effects of κ_0, anelastic attenuation (Q), and magnitude.

Because of the large uncertainty in the data used to develop the NEHRP B/C amplification models evaluated in this study, we suggest that the models based on the Frankel *et al.* (1996), Kamai *et al.* (2013), and R. Kamai *et al.* (unpublished manuscript, 2016; see Data and Resources) velocity profiles (Fea96mod3, Kea13, and Kea16) can be used to represent epistemic uncertainty in the amplification factors. Of the three amplification models developed from the Fea96 velocity profile, we recommend Fea96mod3 should be used for this purpose, because it uses a crustal source velocity (β_S) and a crustal source density (ρ_S) that are more appropriate to WNA crustal properties, and it uses revised densities based on an updated ρ–V_S relationship developed by Boore (2016). Of course, local crustal profiles and corresponding site amplification will vary from these generic crustal models, and we recommend that a site-specific model be used in place of these generic models when one is available.

Data and Resources

The figures were prepared using CoPlot (http://www.cohort.com, last accessed December 2015). SMSIM v.5 was used to perform the stochastic simulations. The latest version of the SMSIM programs can be obtained from http://www.daveboore.com (last accessed December 2015); their use is described in Boore (2005). The digital version of the NEHRP B/C shear-wave velocity profile plotted in figure 2.6 of Kamai *et al.* (2013) was provided by Ronnie Kamai and Walt Silva, and the digital version of the NEHRP B/C shear-wave velocity profile used by R. Kamai *et al.* (unpublished manuscript, 2016) was provided by Ronnie Kamai. This unpublished manuscript "V_{S30} for site response—Why, when, and how?," by R. Kamai, N. A. Abrahamson, and W. J. Silva has been submitted to *Earthquake Spectra*. The unpublished manuscript by A. Zandieh, K. W. Campbell, and S. Pezeshk (2016), "Estimation of κ_0 implied by the high-frequency shape of the NGA-West2 ground motion prediction equations," has been submitted to the *Bulletin of the Seismological Society of America*.

Acknowledgments

Support for the first author was provided by CoreLogic, Inc. We thank Ronnie Kamai and Walt Silva for providing their National Earthquake Hazards Reduction Program (NEHRP) B/C velocity models in digital form and Ronnie Kamai for providing us with a draft of her manuscript. We thank U.S. Geological Survey (USGS) internal reviewers Chuck Mueller and Eric Thompson and external reviewers Ronnie Kamai and Valerio Poggi for their constructive comments that improved the article. We also thank Brad Aagaard and Suzanne Hecker for their helpful editorial comments.

References

Abrahamson, N., W. Silva, and R. Kamai (2014). Summary of the ASK14 ground motion relation for active crustal regions, *Earthq. Spectra* **30,** 1025–1055.

Al Atik, L., A. Kottke, N. Abrahamson, and J. Hollenback (2014). Kappa (κ) scaling of ground-motion prediction equations using an inverse random vibration theory approach, *Bull. Seismol. Soc. Am.* **104,** 336–346.

American Society of Civil Engineers (2013). *Minimum Design Loads for Buildings and Other Structures*, ASCE/SEI 7-10, Reston, Virginia.

Ancheta, T. D., R. B. Darragh, J. P. Stewart, E. Seyhan, W. J. Silva, B. S.-J. Chiou, K. E. Wooddell, R. W. Graves, A. R. Kottke, D. M. Boore, T. Kishida, and J. L. Donahue (2014). PEER NGA-West2 database, *Earthq. Spectra* **30,** 989–1005.

Anderson, J. G., and S. E. Hough (1984). A model for the shape of the Fourier amplitude spectrum of acceleration at high frequencies, *Bull. Seismol. Soc. Am.* **74,** 1969–1993.

Atkinson, G. M., and K. Assatourians (2015). Implementation and validation of EXSIM (a stochastic finite-fault ground-motion simulation algorithm) on the SCEC broadband platform, *Seismol. Res. Lett.* **86,** 48–60.

Atkinson, G. M., and D. M. Boore (2006). Earthquake ground-motion prediction equations for eastern North America, *Bull. Seismol. Soc. Am.* **96,** 2181–2205.

Atkinson, G. M., and W. Silva (2000). Stochastic modeling of California ground motions, *Bull. Seismol. Soc. Am.* **90,** 255–274.

Atkinson, G. M., K. Assatourians, D. M. Boore, K. Campbell, and D. Motazedian (2009). A guide to differences between stochastic point-source and stochastic finite-fault simulations, *Bull. Seismol. Soc. Am.* **99,** 3192–3201.

BC Hydro Engineering (2012). *Dam Safety–Probabilistic Seismic Hazard Analysis (PSHA) Model, Rept. No. E658*, Vols. 1/3**,** Vancouver, British Columbia, Canada.

Beresnev, I. A. (2002). Nonlinearity at California generic soil sites from modeling recent strong-motion data, *Bull. Seismol. Soc. Am.* **92,** 863–870.

Beresnev, I. A., and G. M. Atkinson (2002). Source parameters of earthquakes in eastern and western North America based on finite-fault modeling, *Bull. Seismol. Soc. Am.* **92,** 695–710.

Bonneville, D. R., and A. M. Shuck (2014). An introduction to the 2015 NEHRP recommended seismic provisions for new buildings and other structures, *Proc. of 10th National Conference on Earthquake Engineering*, Anchorage, Alaska, 21–25 July 2014, Paper Number 883, 10 pp.

Boore, D. M. (1983). Stochastic simulation of high-frequency ground motions based on seismological models of the radiated spectra, *Bull. Seismol. Soc. Am.* **73,** 1865–1894.

Boore, D. M. (2003). Prediction of ground motion using the stochastic method, *Pure Appl. Geophys.* **160,** 635–676.

Boore, D. M. (2005). SMSIM—Fortran programs for simulating ground motions from earthquakes: Version 2.3, a revision of OFR 96-80-A, *U.S. Geol. Surv. Open-File Rept. 00-509*, revised 15 August 2005, 55 pp.

Boore, D. M. (2009). Comparing stochastic point-source and finite-source ground-motion simulations: SMSIM and EXSIM, *Bull. Seismol. Soc. Am.* **99,** 3202–3216.

Boore, D. M. (2013). The uses and limitations of the square-root impedance method for computing site amplification, *Bull. Seismol. Soc. Am.* **103,** 2356–2368.

Boore, D. M. (2016). Determining generic velocity and density models for crustal amplification calculations, with an update of the Boore and Joyner (1997) generic site amplification for $\bar{V}_S(Z) = 760$ m/s, *Bull. Seismol. Soc. Am.* **106,** no. 1, doi: 10.1785/0120150229.

Boore, D. M., and C. A. Goulet (2014). The effect of sampling rate and anti-aliasing filters on high-frequency response spectra, *Bull. Earthq. Eng.* **12,** 203–216.

Boore, D. M., and W. B. Joyner (1997). Site amplifications for generic rock sites, *Bull. Seismol. Soc. Am.* **87,** 327–341.

Boore, D. M., and E. M. Thompson (2014). Path durations for use in the stochastic-method simulation of ground motions, *Bull. Seismol. Soc. Am.* **104,** 2541–2552.

Boore, D. M., and E. M. Thompson (2015). Revisions to some parameters used in stochastic-method simulations of ground motion, *Bull. Seismol. Soc. Am.* **105,** 1029–1041.

Boore, D. M., C. Di Alessandro, and N. A. Abrahamson (2014). A generalization of the double-corner-frequency source spectral model and its use in the SCEC BBP Validation Exercise, *Bull. Seismol. Soc. Am.* **104,** 2387–2398.

Boore, D. M., J. P. Stewart, E. Seyhan, and G. M. Atkinson (2014). NGA-West2 equations for predicting PGA, PGV, and 5% damped PSA for shallow crustal earthquakes, *Earthq. Spectra* **30,** 1057–1085.

Bozorgnia, Y., N. A. Abrahamson, L. Al Atik, T. D. Ancheta, G. M. Atkinson, J. W. Baker, A. Baltay, D. M. Boore, K. W. Campbell, B. S.-J. Chiou, R. Darragh, S. Day, J. Donahue, R. W. Graves, N. Gregor, T. Hanks, I. M. Idriss, R. Kamai, T. Kishida, A. Kottke, S. A. Mahin, S. Rezaeian, B. Rowshandel, E. Seyhan, S. Shahi, T. Shantz, W. Silva, P. Spudich, J. P. Stewart, J. Watson-Lamprey, K. Wooddell, and R. Youngs (2014). NGA-West2 research project, *Earthq. Spectra* **30,** 973–987.

Brune, J. (1970). Tectonic stress and the spectra of seismic shear waves from earthquakes, *J. Geophys. Res.* **75,** 4997–5009.

Brune, J. (1971). Correction to "Tectonic stress and the spectra of seismic shear waves", *J. Geophys. Res.* **76,** 5002.

Building Seismic Safety Council (2015). *NEHRP Recommended Seismic Provisions for New Buildings and Other Structures, Part 1 Provisions, Part 2 Commentary, FEMA Rept. No. P-1050-1*, 2015 Edition, Vol. 1**,** National Institute of Building Sciences, Washington, D.C.

Campbell, K. W. (2003). Prediction of strong ground motion using the hybrid empirical method and its use in the development of ground-motion (attenuation) relations in eastern North America, *Bull. Seismol. Soc. Am.* **93,** 1012–1033.

Campbell, K. W. (2004). Erratum to "Prediction of strong ground motion using the hybrid empirical method and its use in the development of ground-motion (attenuation) relations in eastern North America", *Bull. Seismol. Soc. Am.* **94,** 2418.

Campbell, K. W. (2007). *Validation and Update of Hybrid Empirical Ground Motion (Attenuation) Relations for the CEUS*, U.S. Geological Survey NEHRP Award No. 05HQGR0032, Final Technical Report.

Campbell, K. W. (2009). Estimates of shear-wave Q and κ_0 for unconsolidated and semiconsolidated sediments in eastern North America, *Bull. Seismol. Soc. Am.* **99,** 2365–2392.

Campbell, K. W (2011). Ground motion simulation using the hybrid empirical method: Issues and insights, in *Earthquake Data in Engineering Seismology*, S. Akkar, P. Gülkan, and T. van Eck (Editors), Geotechnical, Geological, and Earthquake Engineering, A. Atilla (Series Editor), Vol. 14, Chapter 7, Springer, Berlin, Germany, 81–95.

Campbell, K. W. (2014). An evaluation of eastern North American ground-motion models developed using the hybrid empirical method, *Bull. Seismol. Soc. Am.* **104,** 347–359.

Campbell, K. W., and Y. Bozorgnia (2013). NGA-West2 Campbell–Bozorgnia ground motion model for the horizontal components of PGA, PGV, and 5%-damped elastic pseudo-acceleration response spectra for periods ranging from 0.01 to 10 s, *PEER Rept. No. 2013/06*, Pacific Earthquake Engineering Research Center, University of California, Berkeley, California, 87 pp.

Campbell, K. W., and Y. Bozorgnia (2014). NGA-West2 ground motion model for the average horizontal components of PGA, PGV, and 5% damped linear acceleration response spectra, *Earthq. Spectra* **30,** 1087–1115.

Campbell, K. W., Y. M. A. Hashash, B. Kim, A. R. Kottke, E. M. Rathje, W. J. Silva, and J. P. Stewart (2014). *Reference-rock site conditions for central and eastern North America: Part II—Attenuation (kappa) definition*, *PEER Rept. No. 2014/12*, Pacific Earthquake Engineering Research Center, University of California, Berkeley, California, 54 pp.

Chandler, A. M., N. T. K. Lam, and H. H. Tsang (2006). Near-surface attenuation modelling based on rock shear-wave velocity profile, *Soil Dynam. Earthq. Eng.* **26,** 1004–1014.

Chiou, B. S.-J., and R. R. Youngs (2014). Update of the Chiou and Youngs NGA model for the average horizontal component of peak ground motion and response spectra, *Earthq. Spectra* **30,** 1117–1153.

Douglas, J., and D. M. Boore (2011). High-frequency filtering of strong-motion records, *Bull. Earthq. Eng.* **9,** 395–409.

Drouet, S., F. Cotton, and P. Gueguen (2010). V_{S30}, kappa, regional attenuation and M_w from accelerograms: Application to magnitude 3–5 French earthquakes, *Geophys. J. Int.* **182,** 880–898.

Edwards, B. (2012). *Site Specific Kappa, Rept. No. SED/PRP/R/035b/20120410*, Swiss Federal Institute of Technology, Zürich, Switzerland.

Edwards, B., D. Fäh, and D. Giardini (2011). Attenuation of seismic shear wave energy in Switzerland, *Geophys. J. Int.* **185,** 967–984.

Erdik, M., K. Sestyan, M. B. Demircioglu, C. Tuzun, D. Giardini, L. Gulen, D. S. Akkar, and M. Zare (2012). Assessment of seismic hazard in the Middle East and Caucasus: EMME (earthquake model of Middle East) project, *Proc. of 15th World Conference on Earthquake Engineering*, Lisbon, Portugal, 24–28 September 2012, Paper Number 2100, 10 pp.

European Committee of Standardization (2005). *Eurocode 8: Design of Structures for Earthquake Resistance. Part 1.1: General Rules, Seismic Action and Rules for Buildings*, CEN/TC250-SC8, European Union, Brussels, Belgium.

Frankel, A., C. Mueller, T. Barnhard, D. Perkins, E. Leyendecker, N. Dickman, S. Hanson, and M. Hopper (1996). National seismic hazard maps: Documentation June 1996, *U.S. Geol. Surv. Open-File Rept. 96-532*, 110 pp.

Frankel, A. D., M. D. Petersen, C. S. Mueller, K. M. Haller, R. L. Wheeler, E. V. Leyendecker, R. L. Wesson, S. C. Harmsen, C. H. Cramer, D. M. Perkins, and K. S. Rukstales (2002). Documentation for the 2002 update of the national seismic hazard maps, *U.S. Geol. Surv. Open-File Rept. 2002-420*, 39 pp.

GeoPentech (2015). Southwestern United States ground motion characterization SSHAC level 3, *Technical Report*, Santa Ana, California.

Gupta, A. K. (1993). *Response Spectrum Method in Seismic Analysis and Design of Structures*, CRC Press, Boca Raton, Florida.

Harding, B., C. Tremblay, and D. Cousineau (2014). Standard errors: A review and evaluation of standard error estimators using Monte Carlo simulations, *Quant. Meth. Psychol.* **10,** 107–123.

Hashash, Y. M. A., A. R. Kottke, J. P. Stewart, K. W. Campbell, B. Kim, C. Moss, S. Nikolaou, E. M. Rathje, and W. J. Silva (2014). Reference rock site condition for central and eastern North America, *Bull. Seismol. Soc. Am.* **104,** 684–701.

Idriss, I. M. (2014). An NGA-West2 empirical model for estimating the horizontal spectral values generated by shallow crustal earthquakes, *Earthq. Spectra* **30,** 1155–1177.

International Association for Earthquake Engineering (2012). *Regulations for Seismic Design: A World List–2012*, Tokyo, Japan.

International Code Council (2014). *2015 International Building Code*, Falls Church, Virginia.

Joyner, W. B., R. E. Warrick, and T. E. Fumal (1981). The effect of Quaternary alluvium on strong ground motion in the Coyote Lake, California, earthquake of 1979, *Bull. Seismol. Soc. Am.* **71,** 1333–1349.

Kamai, R., N. A. Abrahamson, and W. J. Silva (2013). *Nonlinear horizontal site response for the NGA-West2 Project*, *PEER Rept. No. 2013/12*, Pacific Earthquake Engineering Research Center, University of California, Berkeley, California.

Kamai, R., N. A. Abrahamson, and W. J. Silva (2014). Nonlinear horizontal site amplification for constraining the NGA-West2 GMPEs, *Earthq. Spectra* **30,** 1223–1240.

Ktenidou, O.-J., F. Cotton, N. Abrahamson, and J. G. Anderson (2014). Taxonomy of kappa: A review of definitions and estimation approaches targeted to applications, *Seismol. Res. Lett.* **85,** 135–146.

Luco, L., R. E. Bachman, C. B. Crouse, J. R. Harris, J. D. Hooper, C. A. Kircher, P. J. Caldwell, and K. R. Rukstales (2015). Updates to building-code maps for the 2015 NEHRP recommended seismic provisions, *Earthq. Spectra* **31,** S245–S271.

Motazedian, D., and G. M. Atkinson (2005). Stochastic finite-fault modeling based on a dynamic corner frequency, *Bull. Seismol. Soc. Am.* **95,** 995–1010.

Pacific Northwest National Laboratory (2014). *Hanford Site-Wide Probabilistic Seismic Hazard Analysis*, Report Number PNNL-23361, Richland, Washington.

Petersen, M., A. Frankel, S. Harmsen, C. Mueller, K. Haller, R. Wheeler, R. Wesson, Y. Zeng, O. Boyd, D. Perkins, N. Luco, E. Field, C. Wills, and K. Rukstales (2008). Documentation for the 2008 update of the United States National Seismic Hazard Maps, *U.S. Geol. Surv. Open-File Rept. 2008-1128*, 128 pp.

Petersen, M. D., M. P. Moschetti, P. M. Powers, C. S. Mueller, K. M. Haller, A. D. Frankel, Y. Zeng, S. Rezaeian, S. C. Harmsen, O. S. Boyd, E. F. Field, R. Chen, K. W. Rukstales, N. Luco, R. L. Wheeler, R. A. Williams, and A. H. Olsen (2014). Documentation for the 2014 update of the United States National Seismic Hazard Maps, *U.S. Geol. Surv. Open-File Rept. 2014-1091*, 243 pp.

Petersen, M. D., M. P. Moschetti, P. M. Powers, C. S. Mueller, K. M. Haller, A. D. Frankel, Y. Zeng, S. Rezaeian, S. C. Harmsen, O. S. Boyd, E. F. Field, R. Chen, K. S. Rukstales, N. Luco, R. L. Wheeler, R. A. Williams, and A. H. Olsen (2015). The 2014 United States National Seismic Hazard Model, *Earthq. Spectra* **31,** S1–S30.

Pezeshk, S., A. Zandieh, K. W. Campbell, and B. Tavakoli (2015). Ground motion prediction equations for CENA using the hybrid empirical method in conjunction with NGA-West2 empirical ground motion models, in *NGA-East: Median Ground Motion Models for the Central and Eastern North America Region*, *PEER Rept. No. 2015/04*, Chapter 5, Pacific Earthquake Engineering Research Center, University of California, Berkeley, California, 119–147.

Pezeshk, S., A. Zandieh, and B. Tavakoli (2011). Hybrid empirical ground-motion prediction equations for eastern North America using NGA models and updated seismological parameters, *Bull. Seismol. Soc. Am.* **101,** 1859–1870.

Poggi, V., B. Edwards, and D. Fäh (2013). Reference *S*-wave velocity profile and attenuation models for ground-motion prediction equations: Application to Japan, *Bull. Seismol. Soc. Am.* **103,** 2645–2656.

Power, M., B. S.-J. Chiou, N. A. Abrahamson, Y. Bozorgnia, T. Shantz, and C. Roblee (2008). An overview of the NGA project, *Earthq. Spectra* **24,** 3–21.

Raoof, M., R. B. Herrmann, and L. Malagnini (1999). Attenuation and excitation of three-component ground motion in southern California, *Bull. Seismol. Soc. Am.* **89,** 888–902.

Rezaeian, S., M. D. Petersen, and M. P. Moschetti (2015). Ground motion models used in the 2014 U.S. National Seismic Hazard Maps, *Earthq. Spectra* **31,** S59–S84.

Rezaeian, S., M. D. Petersen, M. P. Moschetti, P. Power, S. C. Harmsen, and A. D. Frankel (2014). Implementation of NGA-West2 ground motion models in the 2014 U.S. National Seismic Hazard Maps, *Earthq. Spectra* **30,** 1319–1333.

Scherbaum, F., S. Serif, and N. M. Kuehn (2011). On the relationship between Fourier and response spectra: Consequences for the adjustment of empirical ground-motion prediction equations for regional differences, *AGU Fall Meeting Abstracts, American Geophysical Union Fall Meeting*, San Francisco, California, 5–9 December 2011, Vol. 1, Abstract Number S53B–2298.

Seyhan, E., J. P. Stewart, T. D. Ancheta, R. B. Darragh, and R. W. Graves (2014). NGA-West2 site database, *Earthq. Spectra* **30,** 1007–1024.

Silva, W., R. Darragh, N. Gregor, G. Martin, N. Abrahamson, and C. Kircher (1999). *Reassessment of site coefficients and near-fault factors for Building Code Provisions, NEHRP External Research Program*, U.S. Geological Survey NEHRP Award No. 98HQGR1010, Final Technical Report.

Swissnuclear (2013). *PEGASOS Refinement Project–Probabilistic Seismic Hazard Analysis for Swiss Nuclear Power Plant Sites*, Olten, Switzerland.

Tavakoli, B., and S. Pezeshk (2005). Empirical-stochastic ground-motion prediction for eastern North America, *Bull. Seismol. Soc. Am.* **95,** 2283–2296.

Van Houtte, C., S. Drouet, and F. Cotton (2011). Analysis of the origins of κ (kappa) to compute hard rock to rock adjustment factors for GMPEs, *Bull. Seismol. Soc. Am.* **101,** 2926–2941.

Walling, M., W. J. Silva, and N. A. Abrahamson (2008). Non-linear site amplification factors for constraining the NGA models, *Earthq. Spectra* **24,** 243–255.

Woessner, J., D. Giardini, and the SHARE Consortium (2012). Seismic hazard estimates for the Euro-Mediterranean region: A community-based probabilistic seismic hazard assessment, *Proc. of 15th World Conference on Earthquake Engineering*, Lisbon, Portugal, 24–28 September 2012, Paper Number 4337, 10 pp.

Yenier, E., and G. M. Atkinson (2015). An equivalent point-source model for stochastic simulation of earthquake ground motions in California, *Bull. Seismol. Soc. Am.* **105,** 1435–1455.

CoreLogic, Inc.
555 12th Street, Suite 1100
Oakland, California 94607
kcampbell@corelogic.com
(K.W.C.)

U.S. Geological Survey
345 Middlefield Road
Menlo Park, California 94205
boore@usgs.gov
(D.M.B.)

Manuscript received 22 December 2015;
Published Online 16 February 2016